Electronic Supplementary Information

List of Figures and Tables

Fig. S16. ICD spectra of titration of *rac*-[Cr(phen)$_2$dppz](CF$_3$SO$_3$)$_3$ with CT-DNA (150 μM) in 25 mM sodium phosphate buffer (pH=7).

Fig. S17. ICD spectra of titration of Δ-[Cr(phen)$_2$dppz](Cl)$_3$ with CT- DNA (150 μM) in 25 mM sodium phosphate buffer (pH=7).

Fig. S18. ICD spectra of titration of Λ-[Cr(phen)$_2$dppz](Cl)$_3$ with CT- DNA (150 μM) in 25 mM sodium phosphate buffer (pH=7).

Table S1. Crystal data and structural refinement parameters for [Cr(phen)$_2$dppz](CF$_3$SO$_3$)$_3$ and [Cr(phen)$_2$F$_2$dppz](CF$_3$SO$_3$)$_3$.

Table S2. Selected bondlengths (Å) and bondangles (°) of [Cr(phen)$_2$dppz](CF$_3$SO$_3$)$_3$ and [Cr(phen)$_2$F$_2$dppz](CF$_3$SO$_3$)$_3$.

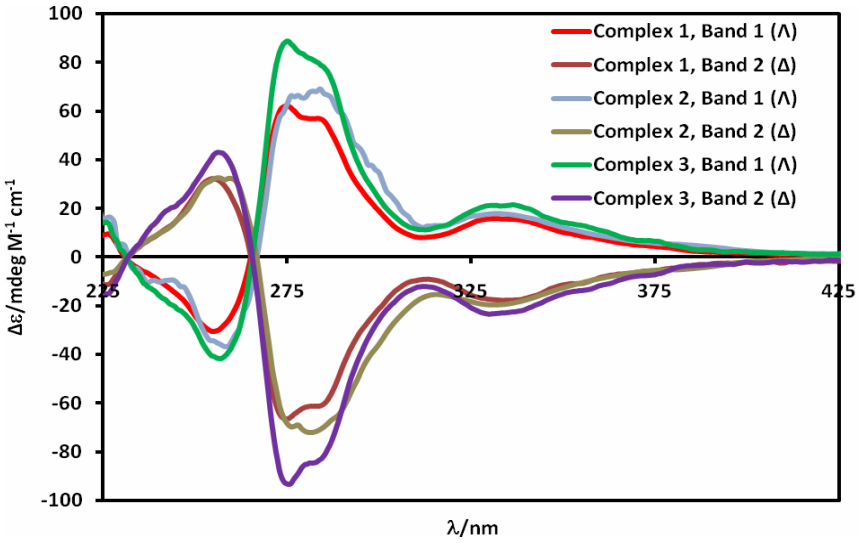

Fig. S1. CD spectra of the Δ and Λ enantiomers of the complexes $[Cr(phen)_2(dppz)](PF_6)_3$ (1), $[Cr(phen)_2(Me_2dppz)](PF_6)_3$ (2) and $[Cr(phen)_2(F_2dppz)](PF_6)_3$ (3) in acetonitrile solution.

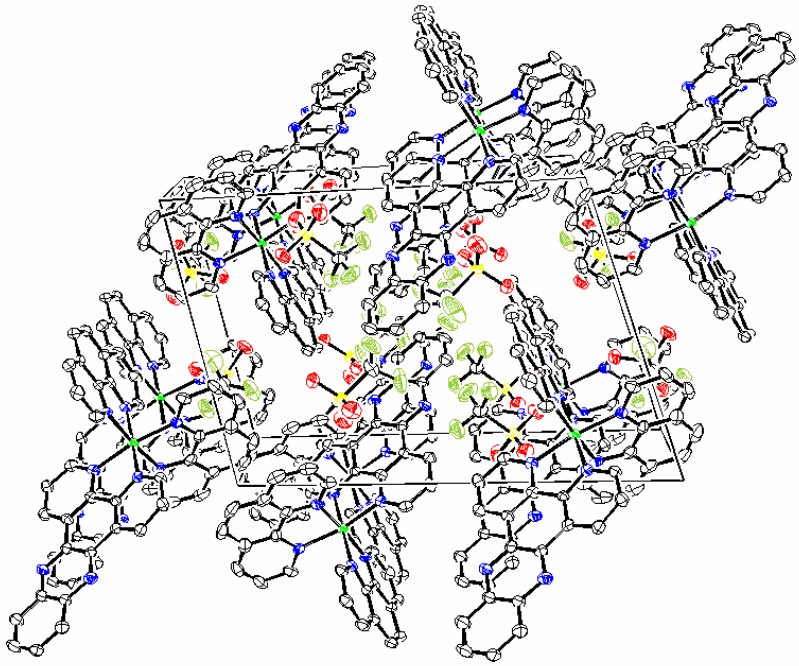

Fig. S2. Packing of $[Cr(phen)_2dppz](CF_3SO_3)_3$ in the unit cell.

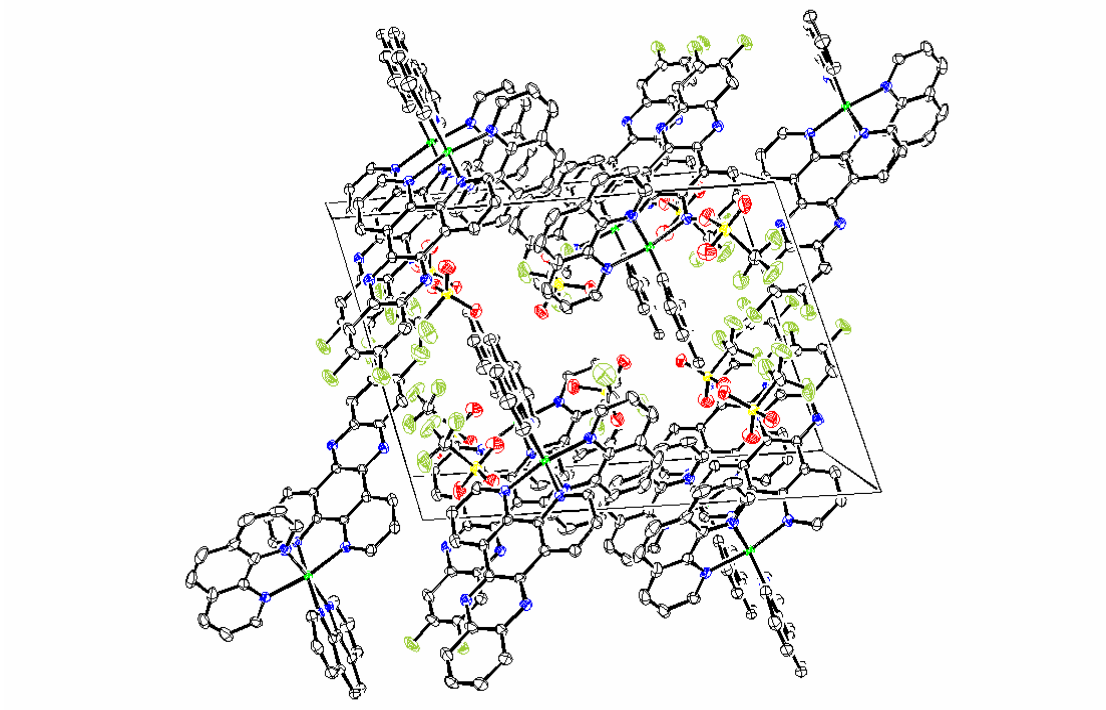

Fig. S3. Packing of $[Cr(phen)_2F_2dppz](CF_3SO_3)_3$ in the unit cell.

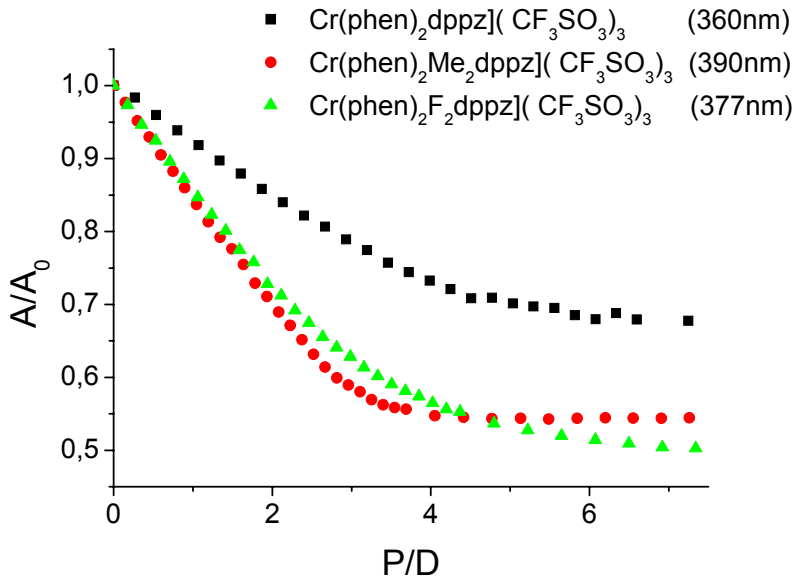

Fig. S4. The comparison of relative absorption intensities (A/A_0) as a function of relative DNA concentration P/D (P/D=[Nucleic Acid]:[Cr]) for $[Cr(phen)_2dppz](CF_3SO_3)_3$

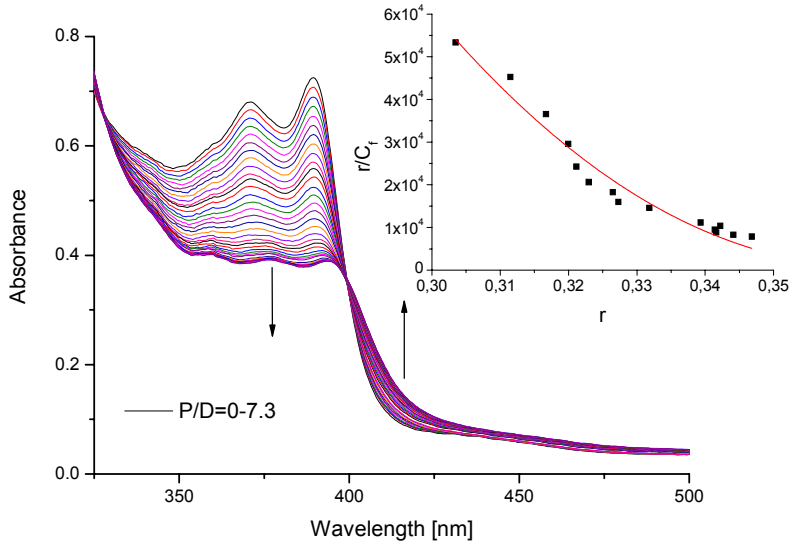

Fig. S5. UV-vis absorption spectra of $[Cr(phen)_2Me_2dppz](CF_3SO_3)_3$ (56 µM in 100mM phosphate buffer solution, pH=7.4) in the presence of increasing concentrations of CT-DNA. Inset: The Scatchard plot for the association of $[Cr(phen)_2Me_2dppz](CF_3SO_3)_3$ with CT-DNA at 390nm. The data were fitted between 20% and 90% bound complexes using the McGhee and von Hippel model.

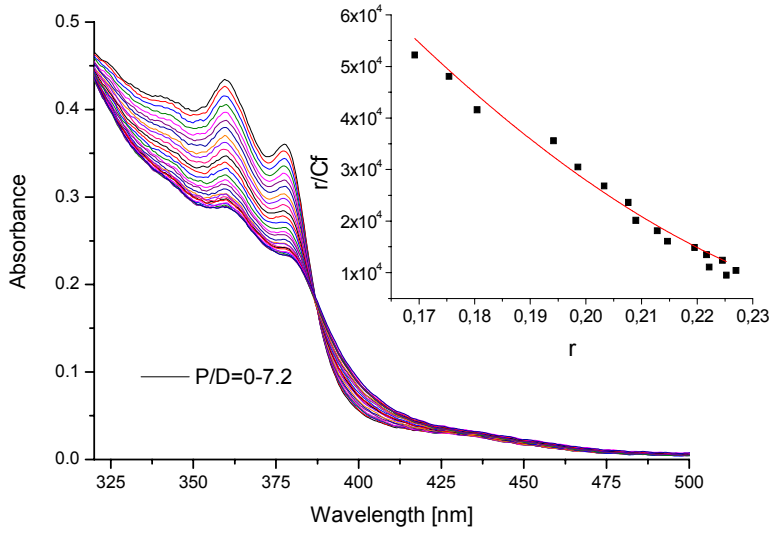

Fig. S6. UV-vis absorption spectra of $[Cr(phen)_2dppz](CF_3SO_3)_3$ (31 µM in 100mM phosphate buffer solution, pH=7.4) in the presence of increasing concentrations of CT-DNA. Inset: The Scatchard plot for the association of $[Cr(phen)_2dppz](CF_3SO_3)_3$ with CT-DNA at 360nm. The data were fitted between 20% and 90% bound complexes using the McGhee and von Hippel model.

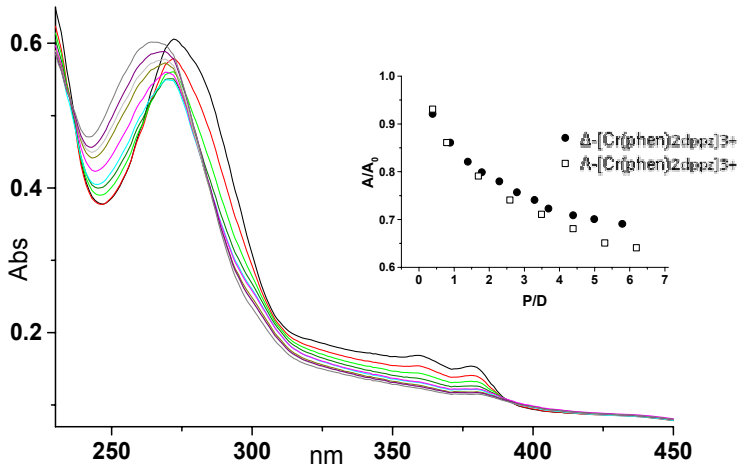

Fig. S7. UV-vis absorption spectra of 25mM phosphate buffer solution (pH=7) of Δ isomer of $[Cr(phen)_2dppz](Cl)_3$ with increasing concentrations of CT-DNA. Inset: A/A_0 plot of Δ and Λ enantiomers

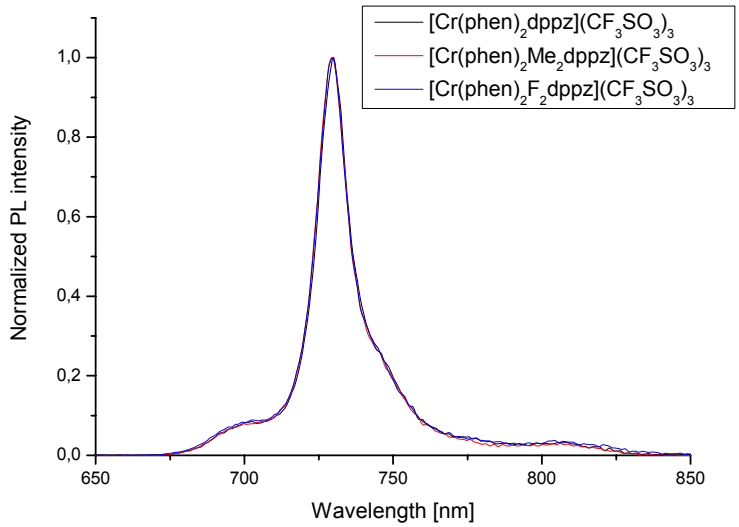

Fig. S8. Normalized emission spectra of $[Cr(phen)_2X_2dppz](CF_3SO_3)_3$ (X=H, Me, F).

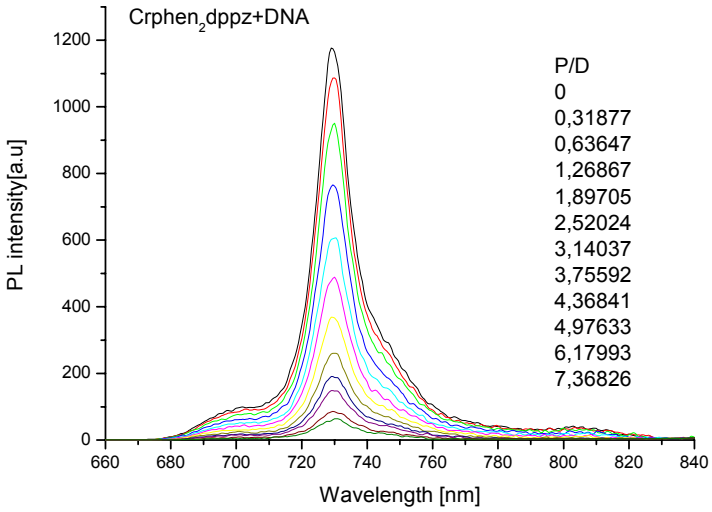

Fig. S9. Phosphorescence spectra of $[Cr(phen)_2dppz](CF_3SO_3)_3$ (65μM in 100mM phosphate buffer solution) in the presence of increasing concentration of CT-DNA.

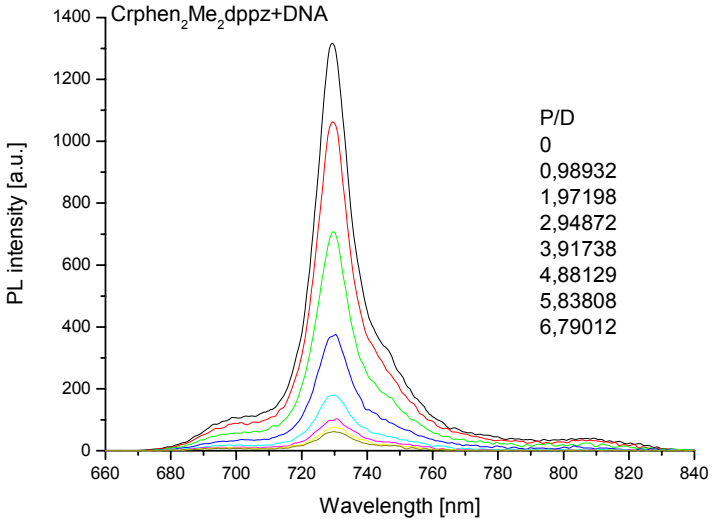

Fig. S10. Phosphorescence spectra of $[Cr(phen)_2Me_2dppz](CF_3SO_3)_3$ (42μM in 100mM phosphate buffer solution) in the presence of increasing concentration of CT-DNA.

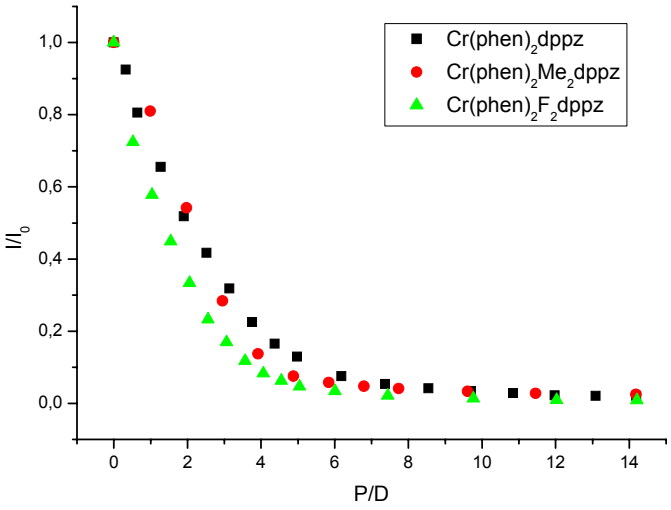

Fig. S11. The quenching of phosphorescence (at 730nm) of Cr(III) dipyridophenazine complexes in the presence of CT-DNA.

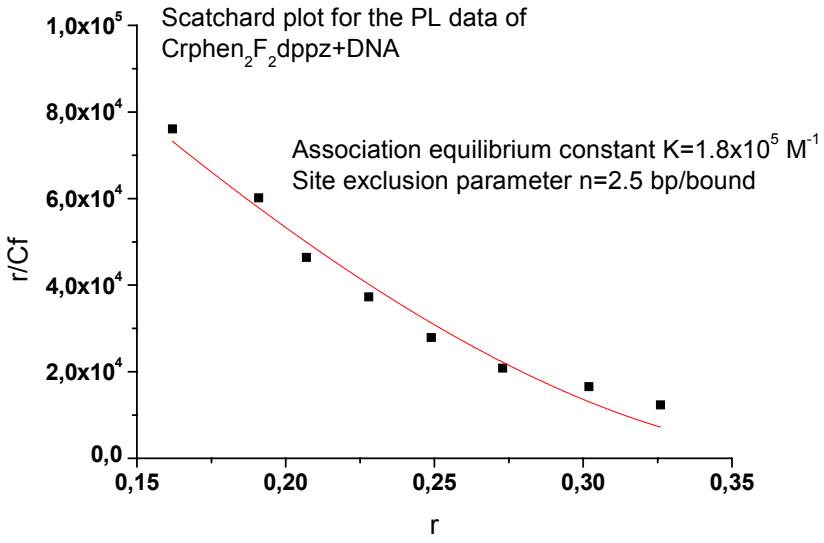

Fig. S12. The Scatchard plot for the association of $[Cr(phen)_2F_2dppz](CF_3SO_3)_3$ with CT-DNA obtained from PL quenching data. The resulting fitting parameters are in very good agreement with those obtained from absorption measurements.

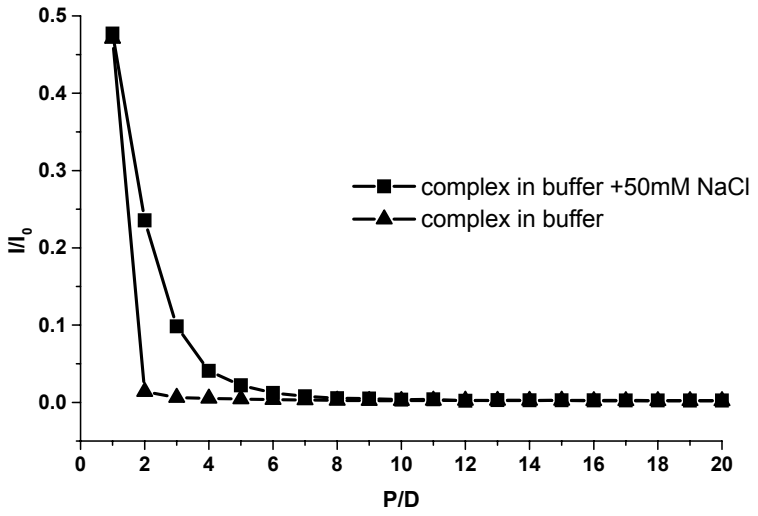

Fig. S13. The effect of [NaCl] on the change in I/I_0 as a function of P/D for the complex $[Cr(phen)_2F_2dppz](CF_3SO_3)_3$, with CT-DNA. [Cr]=16 µM in 10 mM sodium phosphate buffer

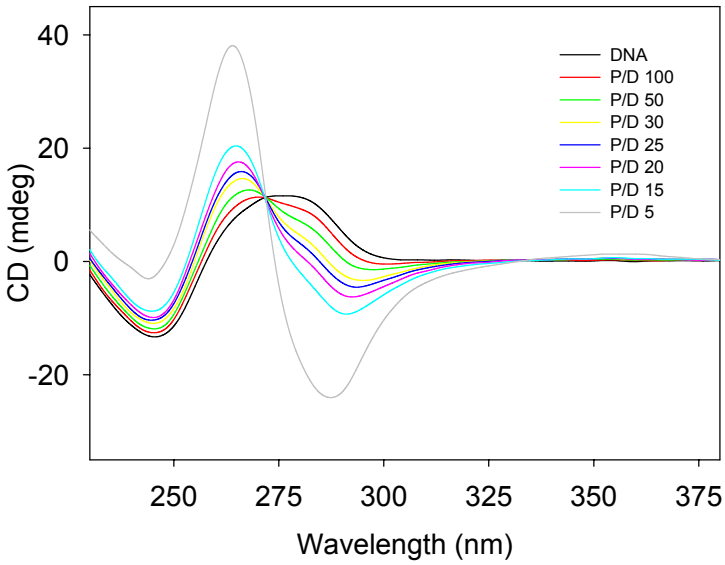

Fig. S14. CD spectra of titration of *rac*-$[Cr(phen)_2dppz](CF_3SO_3)_3$ (55µM) with CT-DNA (150µM) in sodium phosphate buffer (pH=7).

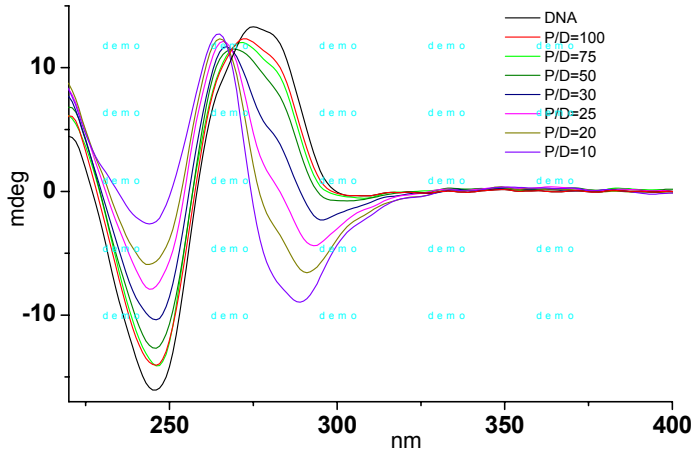

Fig. S15. CD spectra of titration of *rac*-[Cr(phen)$_2$F$_2$dppz](CF$_3$SO$_3$)$_3$ (55µM) with CT-DNA (150 µM) in 25 mM sodium phosphate buffer (pH=7).

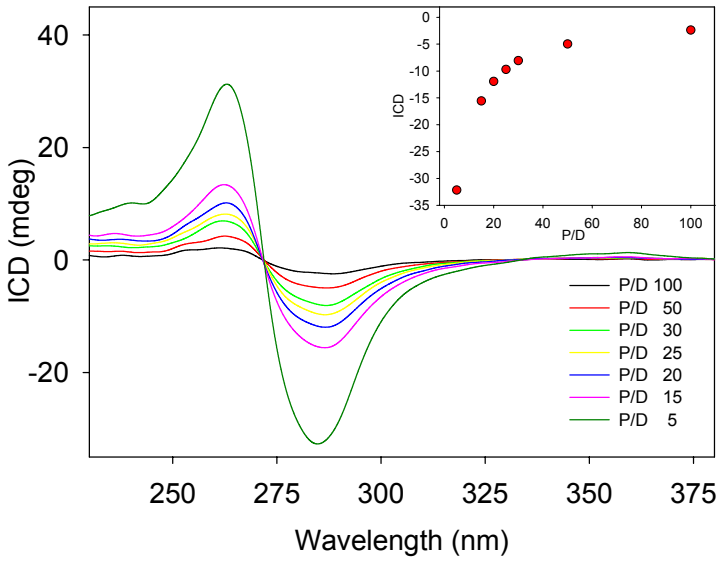

Fig. S16. ICD spectra of titration of *rac*-[Cr(phen)$_2$dppz](CF$_3$SO$_3$)$_3$ with CT-DNA (150 µM) in phosphate buffer (pH=7).

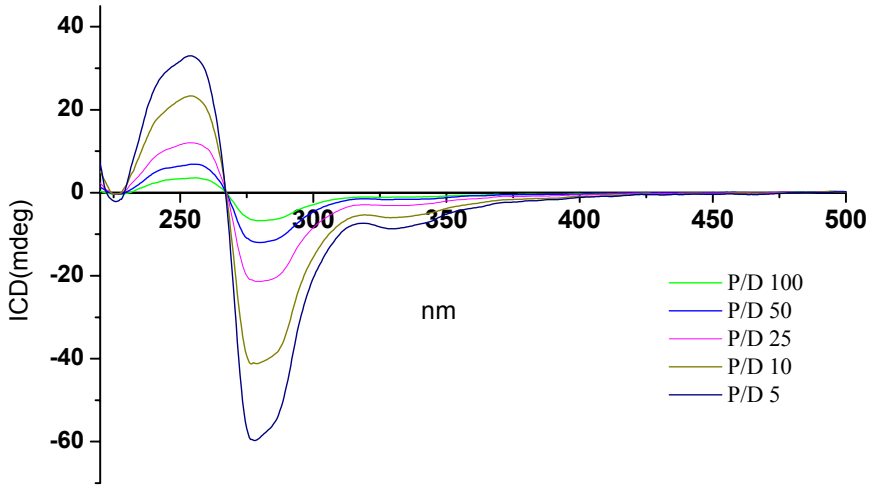

Fig. S17. ICD spectra of titration of Δ-[Cr(phen)$_2$dppz](Cl)$_3$ with CT-DNA (150 µM) in 25 mM sodium phosphate buffer (pH=7).

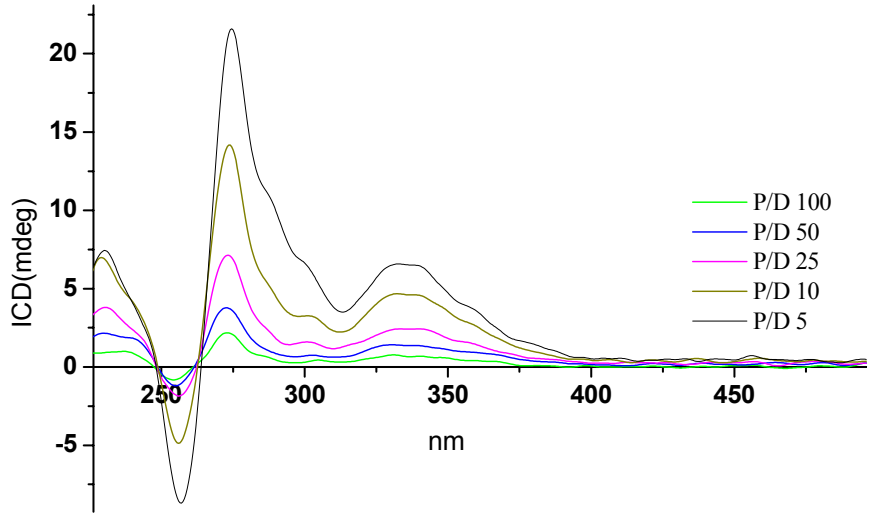

Fig. S18. ICD spectra of titration of Λ-Cr(phen)$_2$dppz](Cl)$_3$ with CT-DNA (150 µM) in 25 mM sodium phosphate buffer (pH=7).

Table S1. Crystal data and structural refinement parameters for $[Cr(phen)_2dppz](CF_3SO_3)_3$ and $[Cr(phen)_2F_2dppz](CF_3SO_3)_3$.

	$[Cr(phen)_2dppz](CF_3SO_3)_3$	$[Cr(phen)_2F_2dppz](CF_3SO_3)_3$
Empirical Formula	$C_{45}H_{26}CrF_9N_8O_9S_3$	$C_{45}H_{24}CrF_{11}N_8O_9S_3$
Formula weight (M)	1141.92	1177.90
Crystal system	Triclinic	Triclinic
Space group	P-1	P-1
Lattice constants a (Å) b (Å) c (Å) α (°) β (°) γ (°)	 10.331(3) 13.214(3) 19.073(5) 72.494(18) 74.473(19) 68.319(15)	 10.2634(14) 13.262(2) 19.284(3) 73.745(7) 74.983(8) 67.915(8)
Volume V($Å^3$)	2271.0(10)	2299.8(6)
Z	2	2
Calculated density (ρ) ($Mg\ m^{-3}$)	1.670	1.701
Absorption coefficient (μ) (mm^{-1})	0.495	0.498
F(000)	1154	1186
θ Range for data collection	2.84 – 25.00	1.12 – 25.00
Limiting Indices	$-12 \le h \le 12$, $-15 \le k \le 15$,$-22 \le l \le 22$	$-12 \le h \le 11$, $-15 \le k \le 15$,$-22 \le l \le 22$
Reflections collected	35508	18396
Unique Reflections	6722 [R_{int}=0.0726]	6379 [R_{int}=0.0339]
Completeness to θ	25 (99.8%)	25 (90.1%)
Data / restraints / parameters	7991/0/677	7288/0/695
Goodness-of-fit on F^2	1.211	1.024
Final R indices [$I > 2\sigma(I)$]	$R_1 = 0.0873$, $wR_2 = 0.1451$	$R_1 = 0.0475$, $wR_2 = 0.1508$
R indices (all data)	$R_1 = 0.1069$, $wR_2 = 0.1531$	$R_1 = 0.0549$, $wR_2 = 0.1769$

Format

Format

Table S2. Selected bondlengths (Å) and bondangles (°) of $[Cr(phen)_2dppz](CF_3SO_3)_3$ and $[Cr(phen)_2F_2dppz](CF_3SO_3)_3$.

$[Cr(phen)_2dppz](CF_3SO_3)_3$		$[Cr(phen)_2F_2dppz](CF_3SO_3)_3$	
Cr1 – N1	2.052(4)	Cr1 – N3	2.051(3)
Cr1 – N2	2.058(4)	Cr1 – N4	2.059(3)
Cr1 – N3	2.062(4)	Cr1 – N5	2.051(3)
Cr1 – N4	2.053(4)	Cr1 – N6	2.056(3)
Cr1 – N5	2.049(4)	Cr1 – N7	2.064(3)
Cr1 – N6	2.059(4)	Cr1 – N8	2.062(3)
N1 – Cr1 – N3	96.19(16)	N6 – Cr1 – N8	80.63(11)
N1 – Cr1 – N4	172.86(16)	N5 – Cr1 – N8	172.55(10)
N1 – Cr1 – N6	94.13(16)	N4 – Cr1 – N8	92.38(10)
N2 – Cr1 – N3	86.95(16)	N6 – Cr1 – N7	86.64(10)
N5 – Cr1 – N6	80.26(16)	N3 – Cr1 – N4	79.77(10)
F1 – C40 – C39	120.1(3)	F1 – C40 – C41	117.4(3)
F2 – C41 – C42	120.1(4)	F2 – C41 – C40	118.1(3)